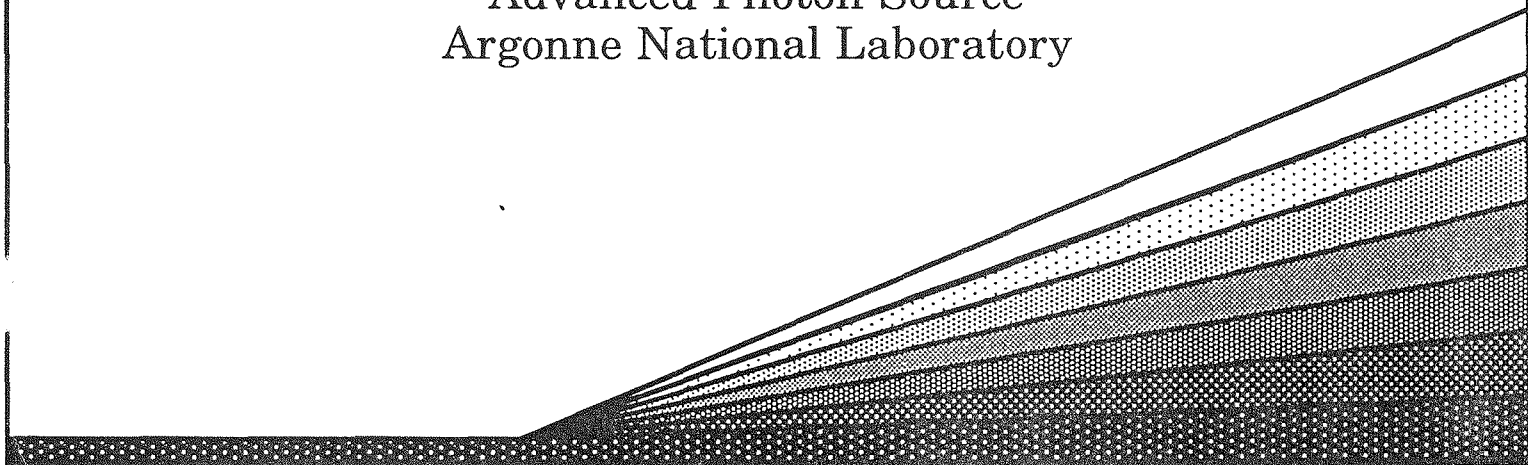


The APS Beamline Front End Vacuum System

R. W. Nielsen
Experimental Facilities Division

October 15, 1993

Advanced Photon Source
Argonne National Laboratory



The APS Beamline Front End
Vacuum System

Robert W. Nielsen

October 13, 1993

Argonne National Laboratory

Advanced Photon Source

Experimental Facilities Division

Table of Contents

	Page
Acknowledgements	ii
Introduction	1
Vacuum Calculations	2
Differential Pump	6
Front End Vacuum Set Points	7
Cleaning Methods and Agents	7
R&D Completed	9
Continuing R&D	10
References	12

Acknowledgements

I would like to acknowledge the following for their help and support in preparation of this paper:

Try Leng Kruey for his hard work, suggestions, and experience in the lab where he has assembled and tested the vacuum systems during the past year.

Deming Shu for his design work of the front end components and the interface to the vacuum components.

The entire design and drafting staff for their drawings and patience during the many changes required to reach the present design.

John Wammack for his efforts in preparing data acquisition systems for the lab work as well as final testing of finished components.

Lester Shirkey for his efforts in designing bakeout and power systems for the vacuum bake cycle.

Dave Ryding for his work on special materials, e.g., tungsten and glidcop to be used in the vacuum system.

Jeff Collins for engineering and coordinating the construction of the clean room facility and to Dave Travis and Dan Nocher for the actual construction.

The members of the Front End Value Engineering Workshop for their recommendations enabling the accomplishment of the desired vacuum criteria more economically.

Tuncer Kuzay for his guidance, constructive criticism, and encouragement.

THE APS BEAMLINE FRONT END VACUUM SYSTEM

Introduction

The APS beamline front ends are designed to be standard, one type for all planned insertion devices (IDs) and another type for all bending magnets (BMs). Depending on the ID source power and user needs, the ID front ends can be of windowless operation (with the use of differential pumps) or of conventional window operation. Figures 1,2, and 3 are drawings of the front end layout for (1) a bending magnet front end, (2) an insertion device front end and (3) a windowless insertion device front end showing the placement of pumps, valves, and required front end hardware. A fast valve is used to protect the storage ring vacuum from the shock wave associated with a massive vacuum breach in the downstream front end or in the downstream beam line proper. This valve is preceded by an all-metal gate valve, which will start to close at the same time the fast valve is triggered. This will isolate the upstream front end and the storage ring vacuum from any further pressure increase caused by downstream vacuum breaches.

Because all the front ends are directly coupled to the storage ring vacuum system, the upstream front end vacuum requirements equal those of the storage ring. This requires a pressure of less than 1 nTorr with beam on. Achieving UHV

vacuum conditions requires that hydrocarbons and contaminants be kept to a minimum. The pumping system will consist of portable dry (oil-free) mechanical pumps backing turbomolecular pumps for roughing the system down and permanently mounted ion pumps with nonevaporable getter capabilities providing the final UHV pumping. Information on UHV pressure will be monitored through the use of nude UHV ion gauges located at upstream and downstream front end locations, and higher pressure information will be obtained through the use of convection gauges located between the fast and slow valve and on the portable roughing carts. Mass spectra will also be monitored at the upstream end of the front ends, where an RGA will be installed.

Vacuum Calculations

The design of the front end vacuum has utilized the finite element analysis computer program developed at Argonne to model and optimize the front end vacuum characteristics. The thermal desorption used for these vacuum calculations is 3×10^{-12} Tl/sec/cm², and the synchrotron-radiation-induced desorption coefficient is 1×10^{-6} molecules/photon after 500 hours of operation with 100 ma circulating positron current in the storage ring. The above thermal desorption value is a standard number used for clean, baked stainless steel.⁽¹⁾ The desorption coefficient (1×10^{-6} mol/photon) is a reasonably attainable value as

agreed upon at an international workshop held at Cornell University.⁽²⁾ The selection and placement of pumps, valves, and bakeout and monitoring equipment are based on the results of the computer analysis.

Figure 1.1 is a bending magnet front end vacuum profile generated by the computer vacuum program depicting 100% of the beam interacting with fixed mask 1. This condition could exist only if gross beam missteering were to occur in the storage ring. It is a worst-case scenario that would be of very short duration because the beam diagnostic feedback system would dump the stored beam.

Figure 1.2 is a bending magnet front end vacuum profile with 10% of the beam interacting with fixed mask 1 and 90% of the beam stopped by shutter 1. This would be the condition of a long-term shutdown of a bending magnet beamline.

Figure 1.3 is a bending magnet front end vacuum profile with 10% of the beam interacting with fixed mask 1, 10% of the beam interacting with fixed mask 2, and 80% of the beam stopped by shutter 2. This would be the condition when users would enter a hutch or beamline area requiring beam to be shut down during entry.

Figure 1.4 is a bending magnet front end vacuum profile with 10% of the beam interacting with fixed mask 1, 10% of the beam interacting with fixed mask 2, 15% interacting with the filters, 10% interacting with the window assembly, and the remainder transported downstream to the user.

From the above (4) examples it can be observed that the necessary vacuum requirements are met in all cases with the exception of that shown in Figure 1.1 in which the upstream vacuum could exceed 1×10^{-9} Torr for a short time until the beam position feedback system either corrects the missteering or shuts down the beam.

Figure 2.1 is an insertion device front end vacuum profile with 100% of the beam interacting with fixed mask 1. This condition could exist only if gross beam missteering were to occur in the storage ring. It is a worst-case scenario that would be of very short duration because the beam diagnostic feedback system would dump the stored beam.

Figure 2.2 is an insertion device front end vacuum profile with 1% of the beam interacting with fixed mask 1 and 99% of the beam stopped by shutter 1. This would be the condition of a long-term shutdown of an insertion device front end.

Figure 2.3 is an insertion device front end vacuum profile with 1% of the beam interacting with fixed mask 1, 1% interacting with fixed mask 2, and 98% of the beam stopped on shutter 2. This would be the condition during which users would enter hutches or other areas requiring beam to be off.

Figure 2.4 is an insertion device front end vacuum profile with 1% of the beam interacting with each of fixed masks 1 and 2, 3% interacting with shutter 2, 5% interacting

with the filters, 1.5% interacting with the exit window, and the remainder transported to the users.

From the above (4) examples it can be observed that the necessary vacuum requirements are met in all cases with the exception of that shown in Figure 2.1 in which the upstream vacuum could exceed 1×10^{-9} Torr for a short time until the beam position feedback system either corrects the missteering or shuts down the beam.

Figure 3.1 is a windowless insertion device front end vacuum profile with the same conditions as in Figure 2.1 above.

Figure 3.2 is a windowless insertion device front end vacuum profile with the same conditions as in Figure 2.2 above.

Figure 3.3 is a windowless insertion device front end vacuum profile with conditions equal to those in Figure 2.3 above.

Figure 3.4 is a windowless insertion device front end vacuum profile with conditions similar to those in Figure 2.4 above. The difference is due to the differential pump negating the need for filters and the window assemblies. The beam interaction with these components is eliminated.

From the above (4) examples it can be observed that the necessary vacuum requirements are met in all cases with the exception of that shown in Figure 3.1 in which the upstream vacuum could exceed 1×10^{-9} Torr for a short time until the

beam position feedback system either corrects the missteering or shuts down the beam.

Differential Pump

Figure 4 is a diagram of the standard differential pump designed for APS operation. Using apertures of 10mm x 78mm, 12mm x 78mm and 14mm x 78mm (as shown in the drawing), pressure differentials of greater than two orders of magnitude have been obtained. An added benefit has been the time delay observed when producing a high pressure burst at the downstream end of the pump and measuring the time before the pressure increase is detected on the upstream end of the pump. Figure 5 is a plot showing this measured delay when allowing the downstream pressure to rise rapidly from 2.4×10^{-7} Torr to 1×10^{-4} Torr. A delay in excess of 100 msec is evident. Other delays are engineered into the front ends in the form of small apertures on each side of large volume chambers. Figures 6 and 7 show the aperture sizes and locations for an insertion device front end and a front end specifically for undulators, respectively. Formal delay line tubes are included in the bending magnet front end as well as in the windowless insertion device front end. No space is available for a formal delay line in the conventional window-type insertion device front end.

Front End Vacuum Set Points

All front ends are equipped with valving and vacuum sensing to protect the storage ring vacuum in the event of a severe vacuum breach in a beamline. Figure 8 is a diagram showing the logic and set points used to control three valves (SV, slow valve), (FV, fast valve) and (EV, exit valve) to protect and isolate various sections of the front-end and the storage ring. In order for the EV to open, the pressure downstream of the differential pump must be $< 1 \times 10^{-6}$ Torr, and the pressure upstream of the differential pump must be $< 1 \times 10^{-8}$ Torr, and the pressure in the safety shutter chamber must be $< 6 \times 10^{-9}$ Torr. Any one of the three pressures exceeding their set point will cause the EV to close or prevent it from opening. If the pressure upstream of the EV reaches 1×10^{-8} Torr or higher, the SV will close as will shutter 1 to prevent beam from damaging the valve. If the pressure upstream of the EV reaches or exceeds 1×10^{-5} Torr, the SV and the FV will close and beam in the storage ring will be dumped. This will happen only if a serious pressure problem exists in the beamline.

Cleaning Methods and Agents

New cleaning techniques have been investigated to comply with ES&H and to reduce cleaning waste and residue, disposal of which is very expensive. One product tested is

Citronox, which is a citric-acid-based product and can be disposed of by flushing down the drain. This product has been used in a 5% solution with DI water at 55 deg. C to clean copper and glidcop samples. A 15-minute bath in Citronox has cleaned these materials but has left a brownish oxide layer, which was removed by scrubbing with scotchbrite pads with trichlor, acetone, and methanol. Glidcop processed in this manner has been installed in a vacuum system and pumped into the mid 10^{-11} Torr range with no undesirable traces detected on an RGA.

A novel method of cleaning using supercritical CO₂ has been examined with some encouraging results.⁽³⁾ Supercritical cleaning relates to the properties of gas liquification. If a pure gas is compressed below a "critical temperature," liquification occurs. At temperatures above the critical temperature no liquification is possible regardless of the pressure applied. Figure 9 is a phase diagram of a typical supercritical fluid. For CO₂, the critical temperature is 31 deg. C and the critical pressure is 1073 psi. As the pressure is increased, the gas density increases to near-liquid density at which point the supercritical fluid displays good solubilizing properties. The cleaning effectiveness of supercritical CO₂ is dependent on the temperature, pressure, flow rate, turbulence, and time left in the media. The bottom diagram in Figure 9 is a schematic of a supercritical cleaning system. Samples of

stainless steel, copper, and glidcop were cleaned with this method, and the results compared with cleaning in trichlor, acetone, and methanol using ultrasonics. Figure 10 is a sample ESCA plot, which was the method used to analyze the results. Figure 11 is a chart of the results showing that the chemical cleaning results are somewhat better than the supercritical results. During the supercritical cleaning, the flow rate was so low that no turbulence was present. It is believed that increasing the flow rate and adding ultrasonics or agitation could improve the effectiveness of this cleaning method. Testing will continue.

R&D Completed

Testing has been completed on a 4" fast valve of the type to be used to protect the storage ring vacuum from vacuum breaches in a beamline or downstream front end. The top diagram of Figure 12 shows the experimental setup used to test the valve closing time. A laser was directed through the windows on each side of the valve to a detector on the opposite side of the valve. The center plot of Figure 12 is an oscilloscope trace showing the closing time (6.3 msec) when the valve was closed by pushing the close button on the controller. The bottom plot of Figure 12 shows the closing time when the pressure was increased above the set point in the chamber containing the valve pressure sensor (cold

cathode gauge). The closing time was 6.76 msec. Well over 100 cycles were run with no apparent change in closing time.

Work has been done on developing a UHV-compatible tungsten in which porosity is minimized to reduce thermal desorption gas loads. Measurements of tungsten outgassing has been done at Berkeley at the ALS.⁽⁴⁾ The results from Berkeley were .87 nTorr l/sec/cm² from an 85 cm² surface area sample. The sample measured at the APS using a 690 cm² sample yielded a .22 nTorr l/sec/cm² thermal desorption. The desorption for clean baked stainless steel is .01 nTorr l/sec/cm². The sample used at the APS was type HD18DS from Mi-Tech Metals. This sample was first cleaned by scrubbing with Scotchbrite in trichlor, acetone, and methanol and was then cleaned ultrasonically in each of these agents for 15 min. This block of tungsten was put in a vacuum system and pumped to 6×10^{-11} Torr with no adverse elements in the RGA spectra. Comparable samples have also been supplied by Kulite Corp. Both manufacturers now supply UHV-grade tungsten.

Continuing R&D

A full-scale prototype windowless front end is being constructed and assembled in the building 362 high bay where several vacuum as well as other tests will be conducted. Planned vacuum tests include (1) determination of front end roughing time and pump-down time, (2) measurement of the

front end vacuum profile, (3) shock-wave delay measurements and (4) measurement of the pressure in the upstream front-end area after breaking a downstream window and allowing the entire safety system (FV,SV, etc.)to shut down the front end vacuum system.

References

1. A. Roth, *Vacuum Technology* (Second Edition) p.144
2. "Workshop Summaries from the International Workshop on Vacuum Systems for B-Factories and High-Energy Synchrotron Light Sources," Cornell University, January 16 - 18, 1992, CLNS92/1134
3. R. Nielsen and T.M.Kuzay, "Preliminary Cleaning Tests on Candidate Materials for APS Beamline and Front End Components," May 12, 1992, LS-197
4. Thomas Swain, "UHV Issues for Tungsten Radiation Stops," March 4, 1991, AL-20-15

BM Front End Vacuum Profile With 100% of Beam on Fixed Mask 1

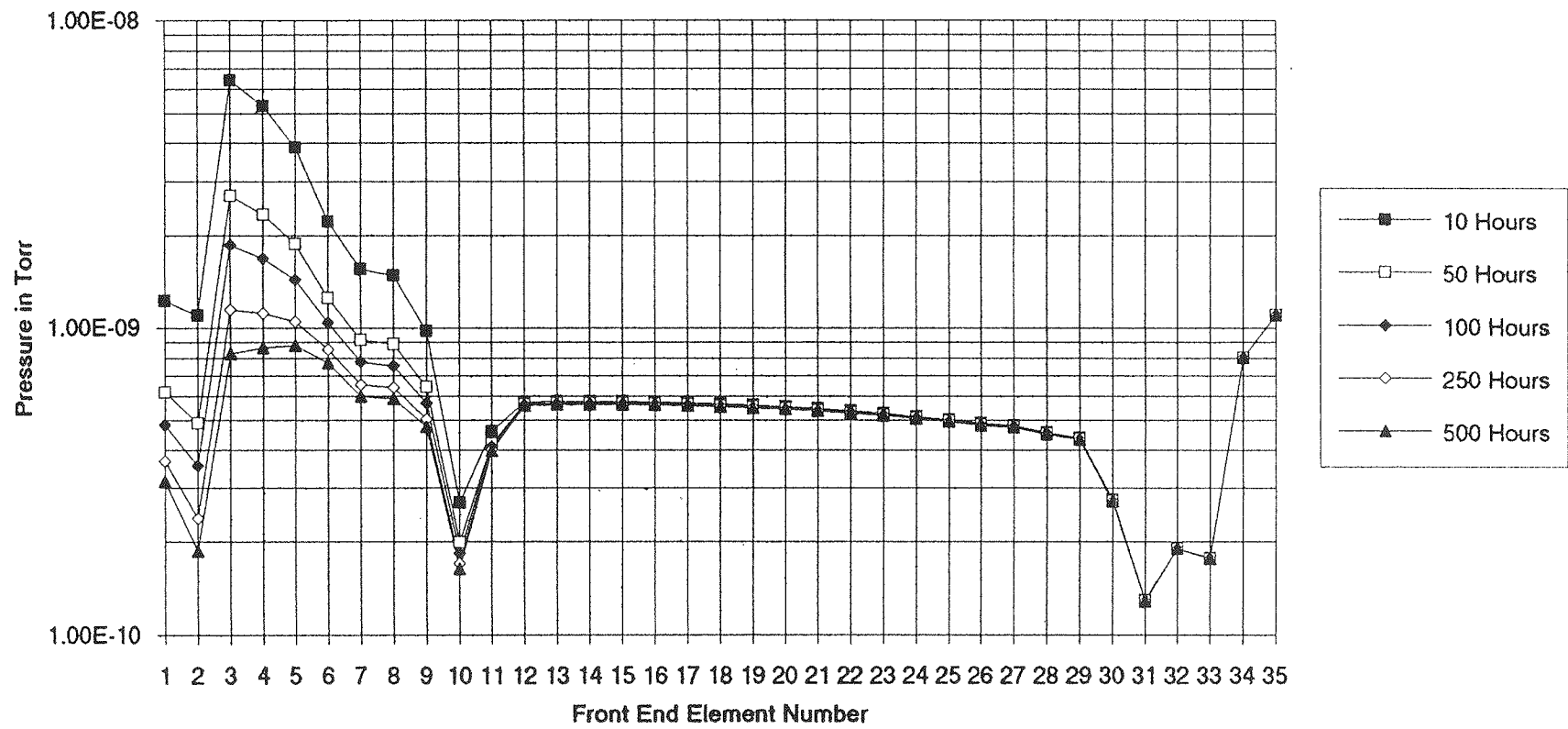


Figure 1.1

Bm Front End Vacuum Profile With 10% Beam on Fixed mask 1 & 90% Beam on Shutter 1

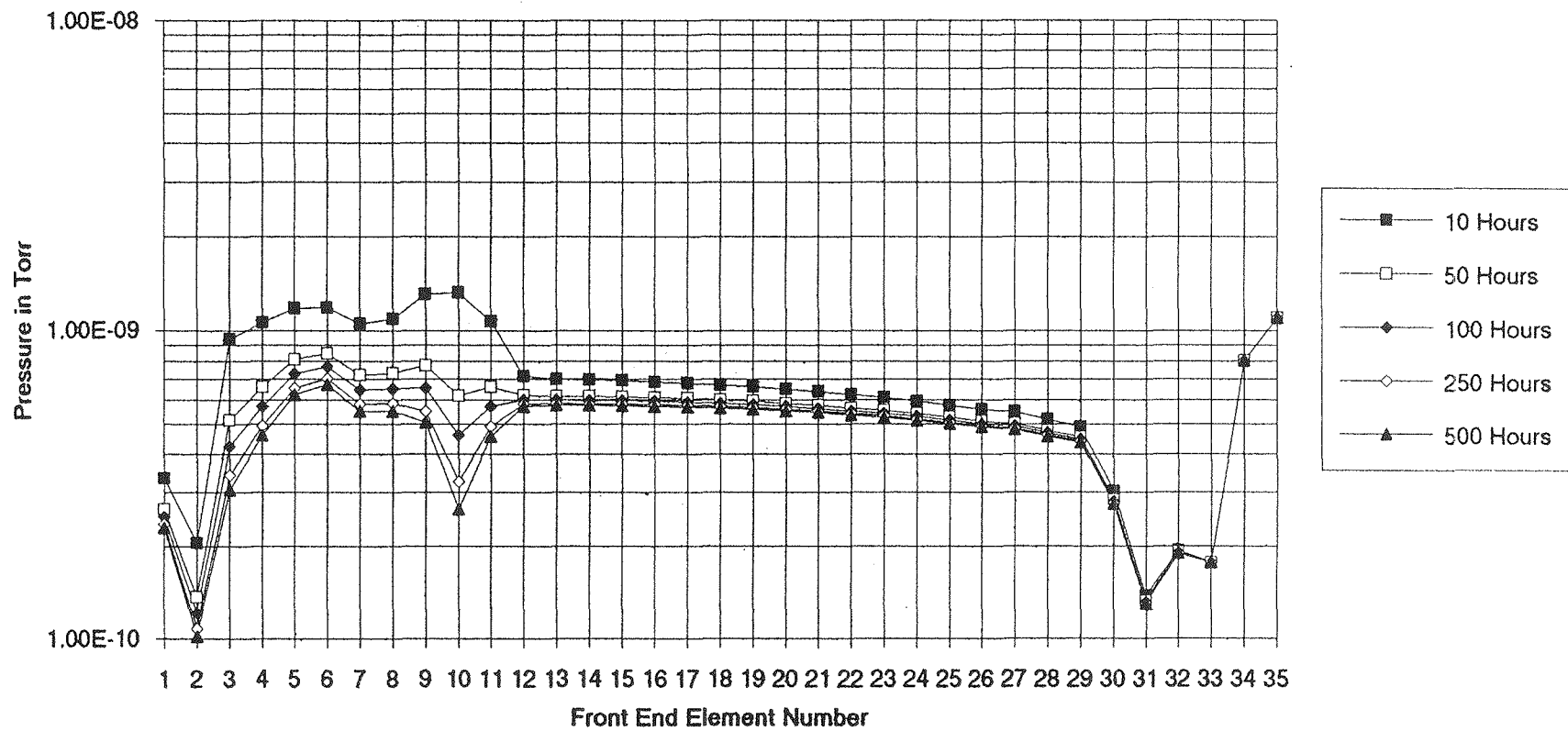


Figure 1.2

BM Front End Vacuum Profile With 10% Beam on FM1, 10% Beam on FM2, & 80% Beam on Shutter 2

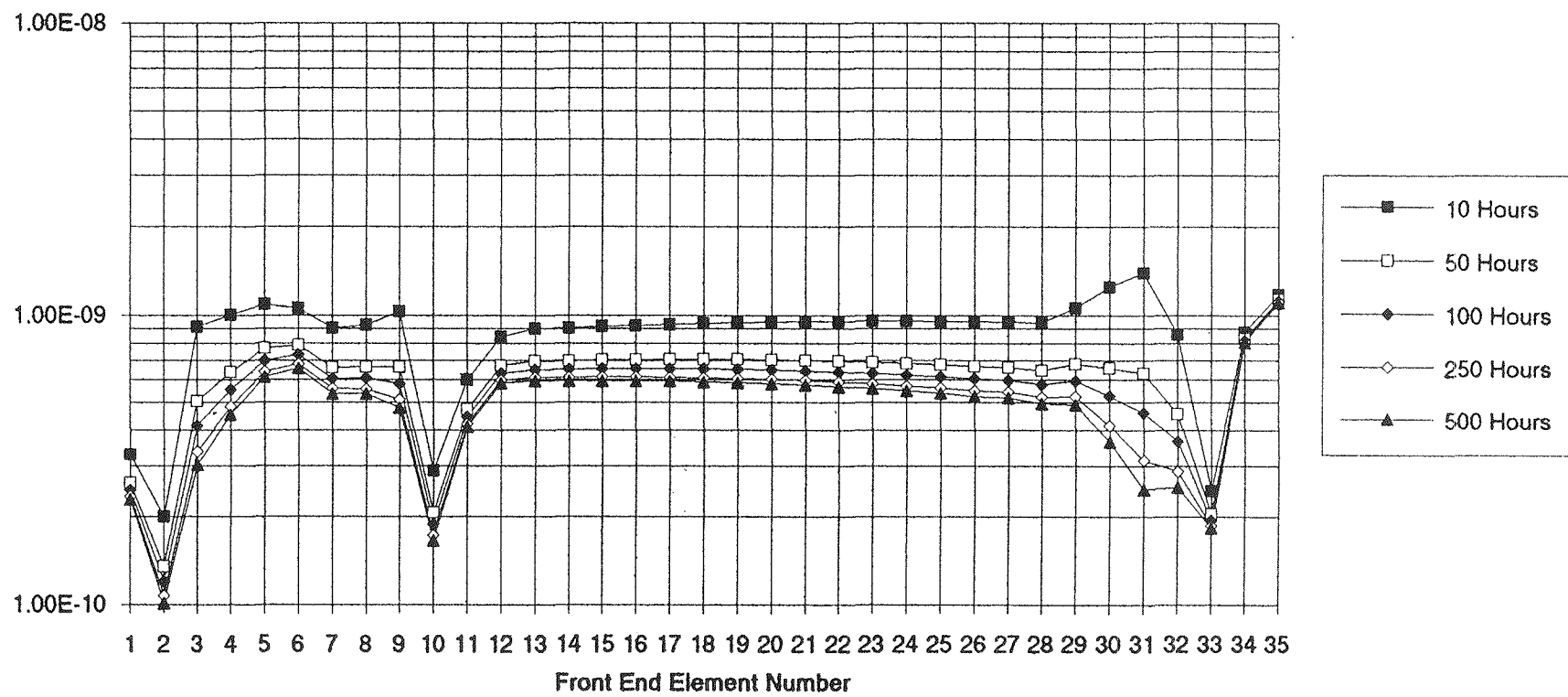


Figure 1.3

BM Front End Vacuum Profile With 10% Beam on FM1, 10% on FM2, 15% on Filters, & 10% on Windows

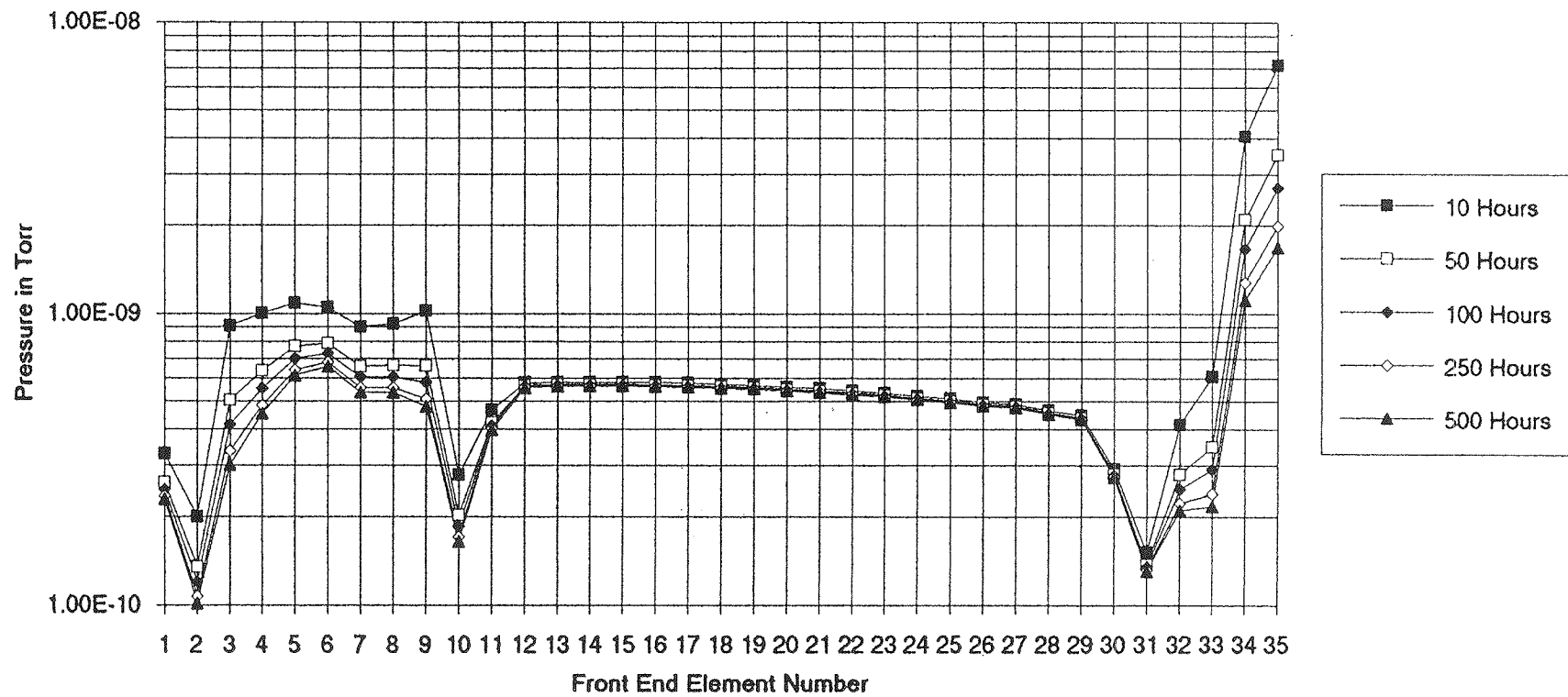


Figure 1.4

ID Front End Vacuum Profile With 100% Beam on FM1

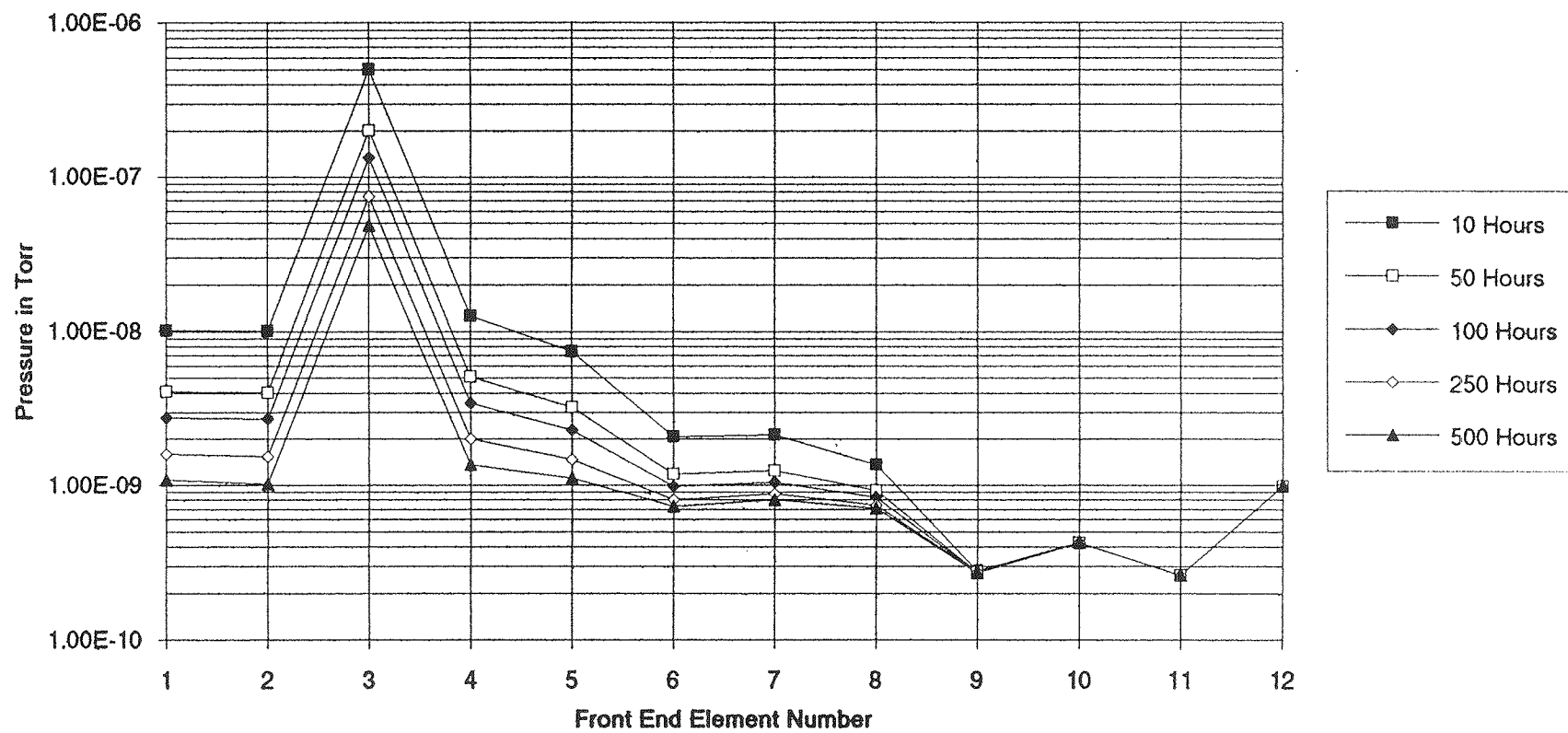


Figure 2.1

ID Front End Vacuum Profile With 1% Beam on FM1 & 99% Beam on Shutter 1

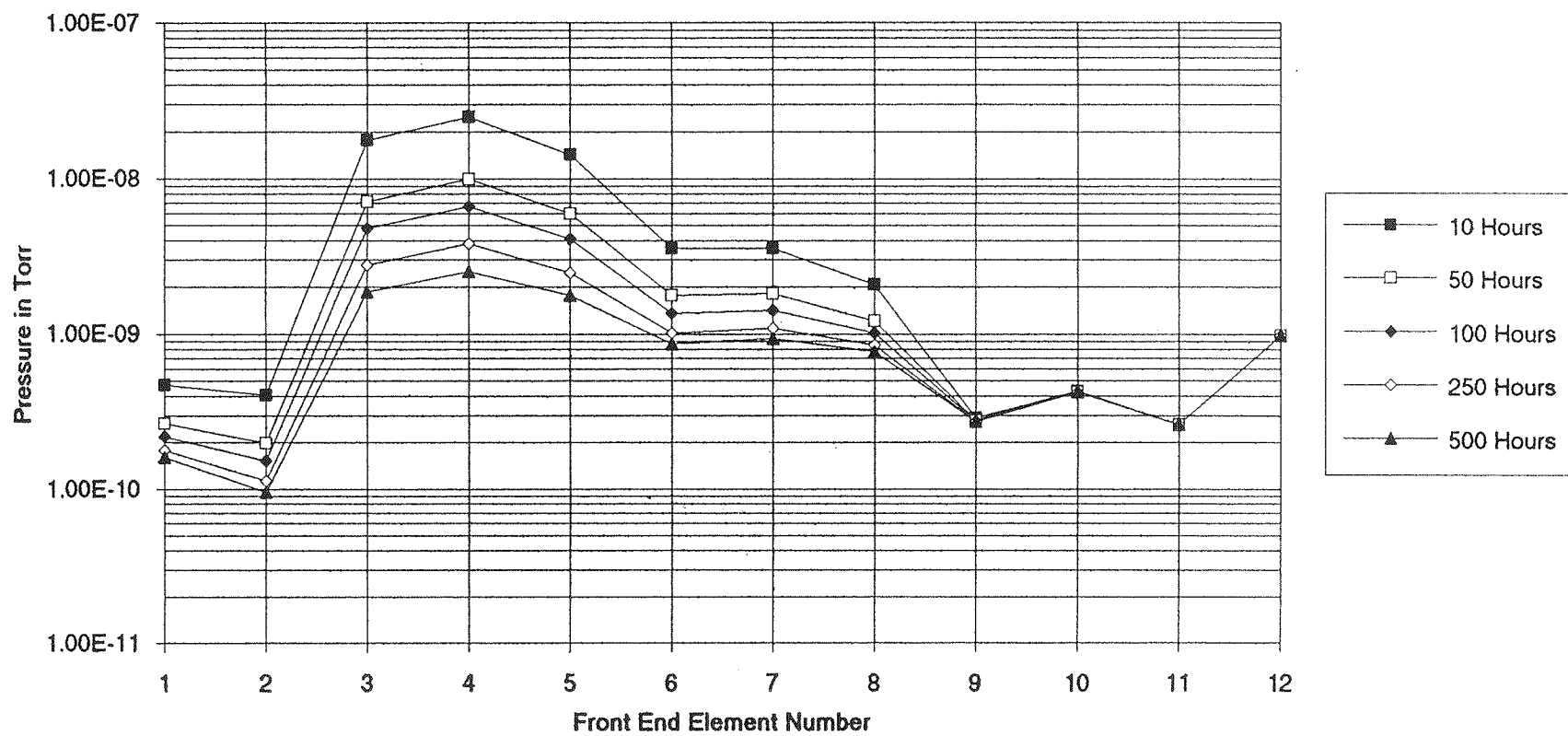


Figure 2.2

ID Front End Vacuum Profile With 1% Beam on FM1, 1% Beam on FM2, & 98% Beam on Shutter 2

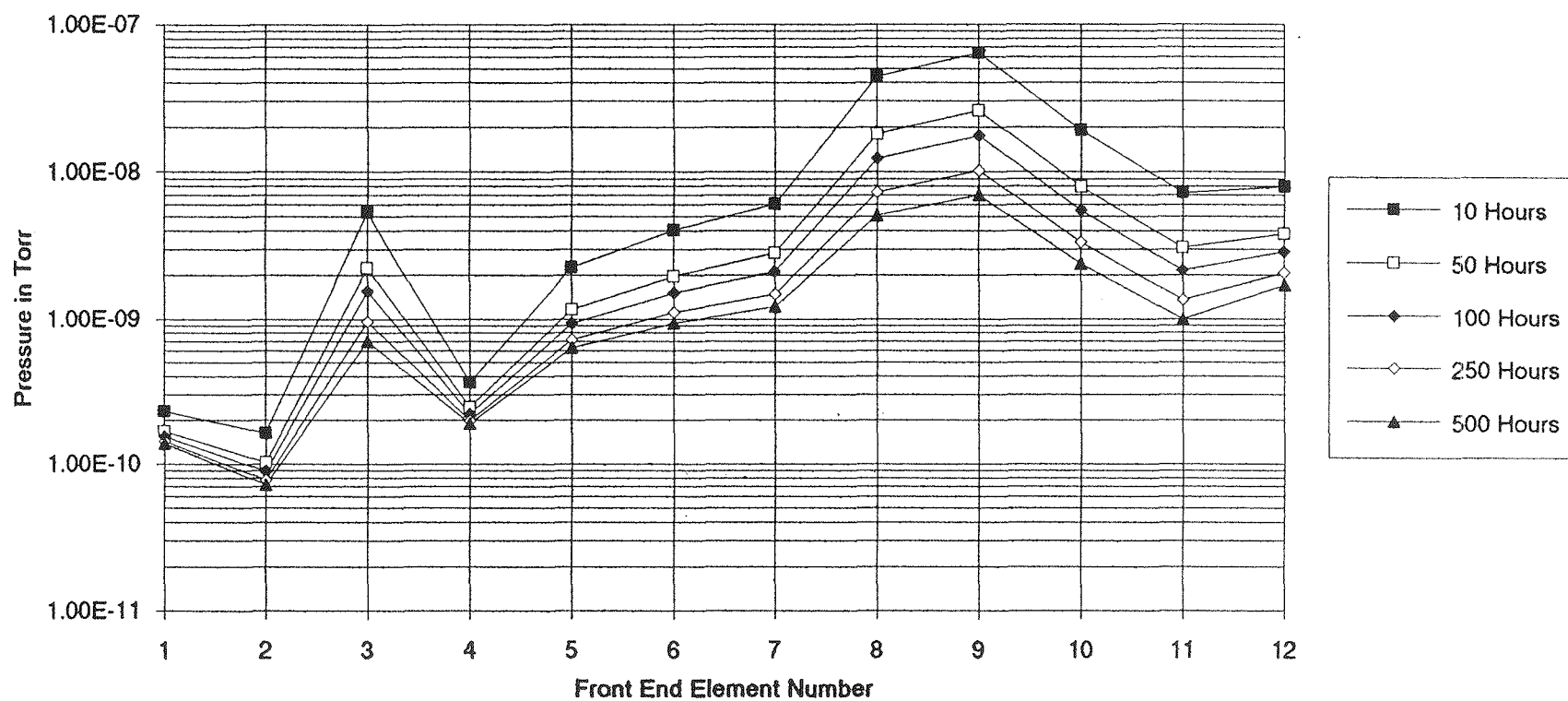


Figure 2.3

ID Front End Vacuum Profile With 1% Beam on FM1&2, 3% Beam on Shutter 2, 5% Beam on Filters, & 1.5% Beam on Exit Window

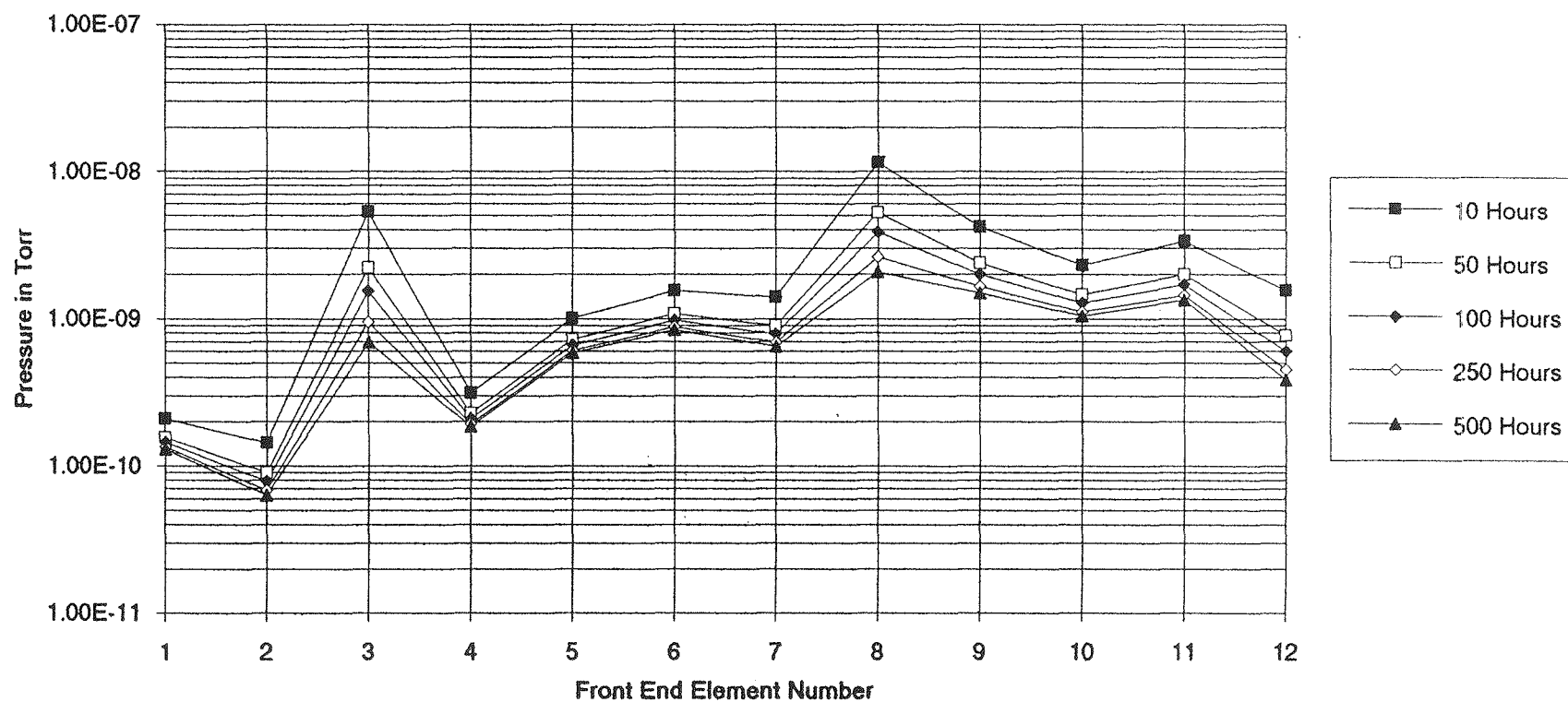


Figure 2.4

Windowless ID Front End Vacuum Profile With 100% of Beam on FM1

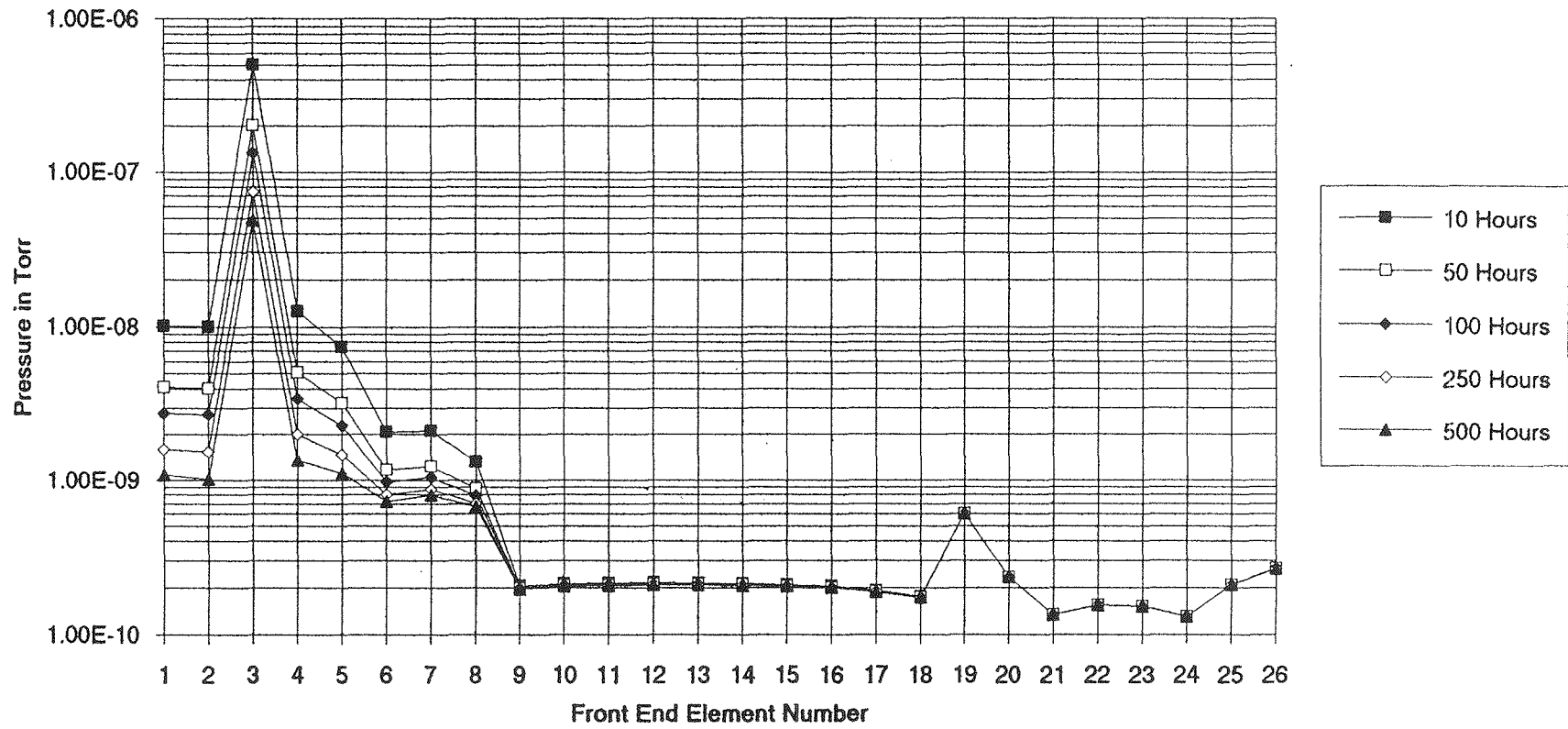


Figure 3.1

Windowless ID Front End Vacuum Profile With 1% Beam on FM1 & 99% Beam on Shutter 1

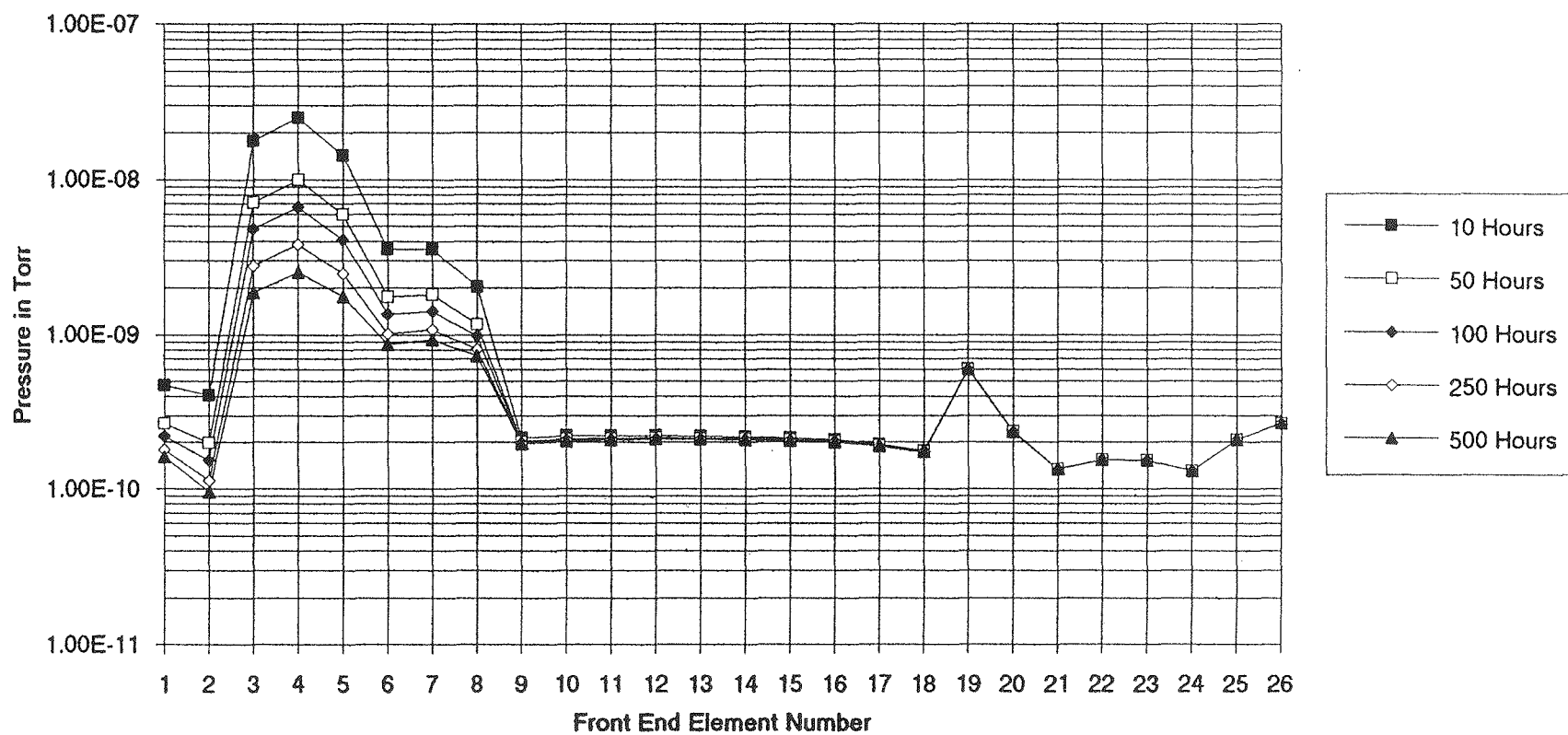


Figure 3.2

Windowless ID Front End Vacuum Profile With 1% Beam on FM1, 1% Beam on FM2, & 98% Beam on Shutter 2

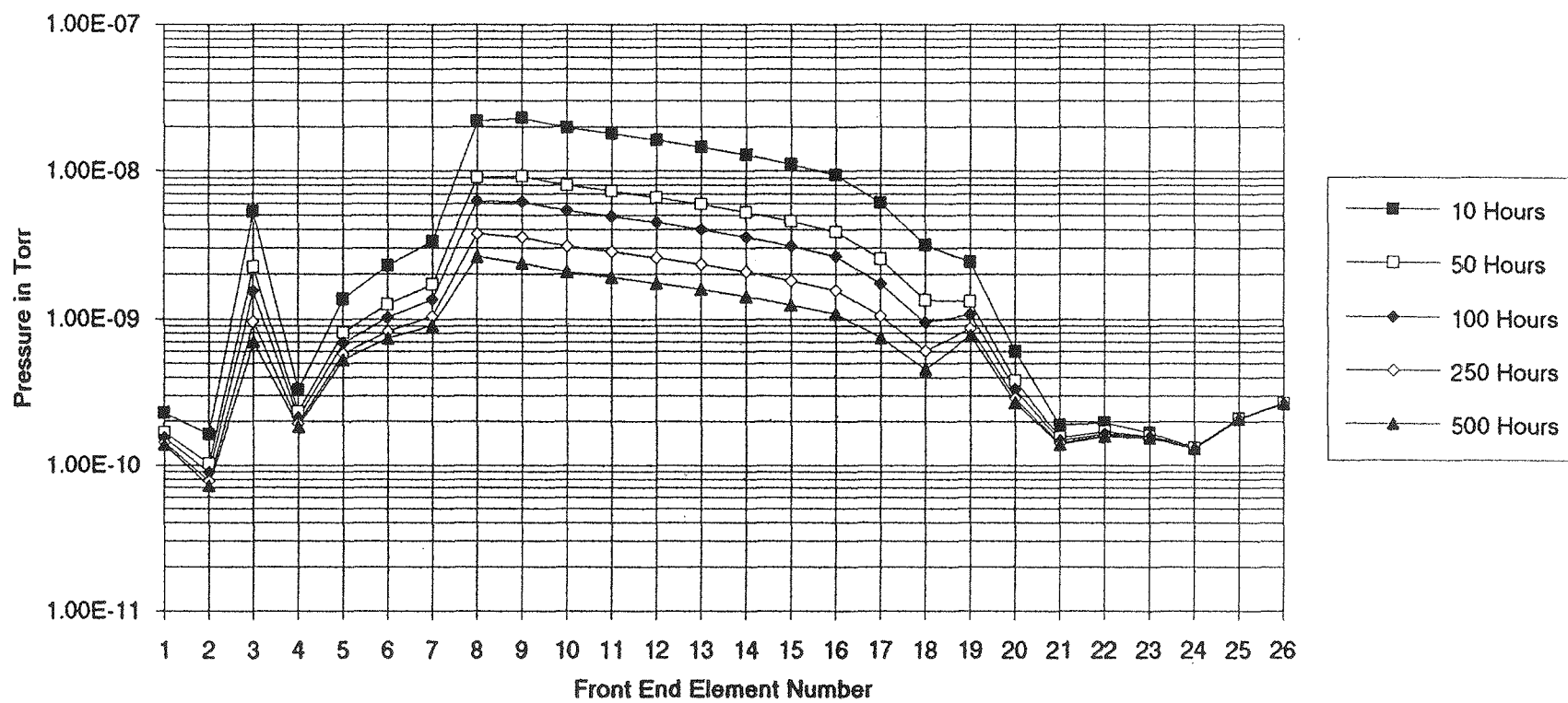


Figure 3.3

Windowless ID Front End Vacuum Profile With 1% Beam on FM1, 1% Beam on FM2, & 3% Beam on Shutter 2. Remainder of Beam to User.

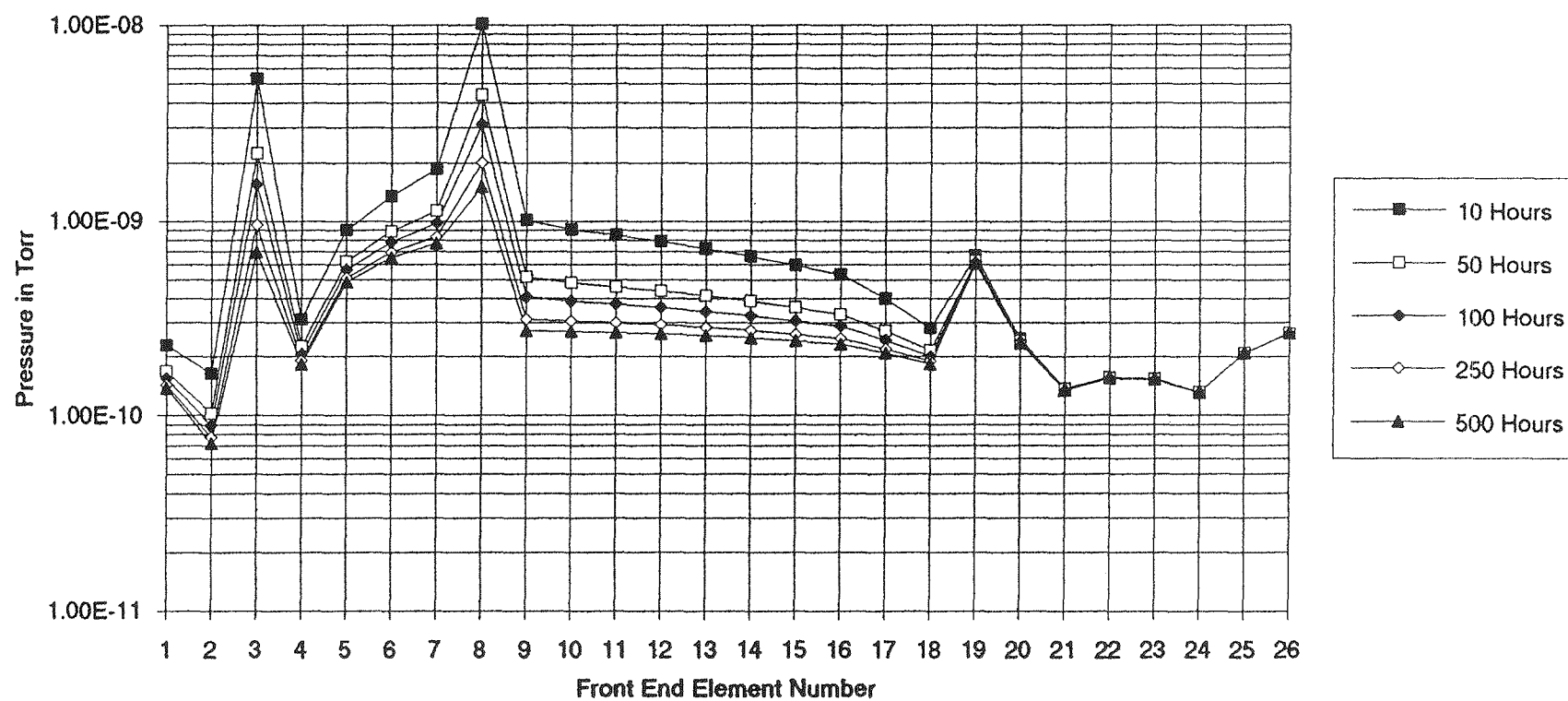


Figure 3.4

Figure 4

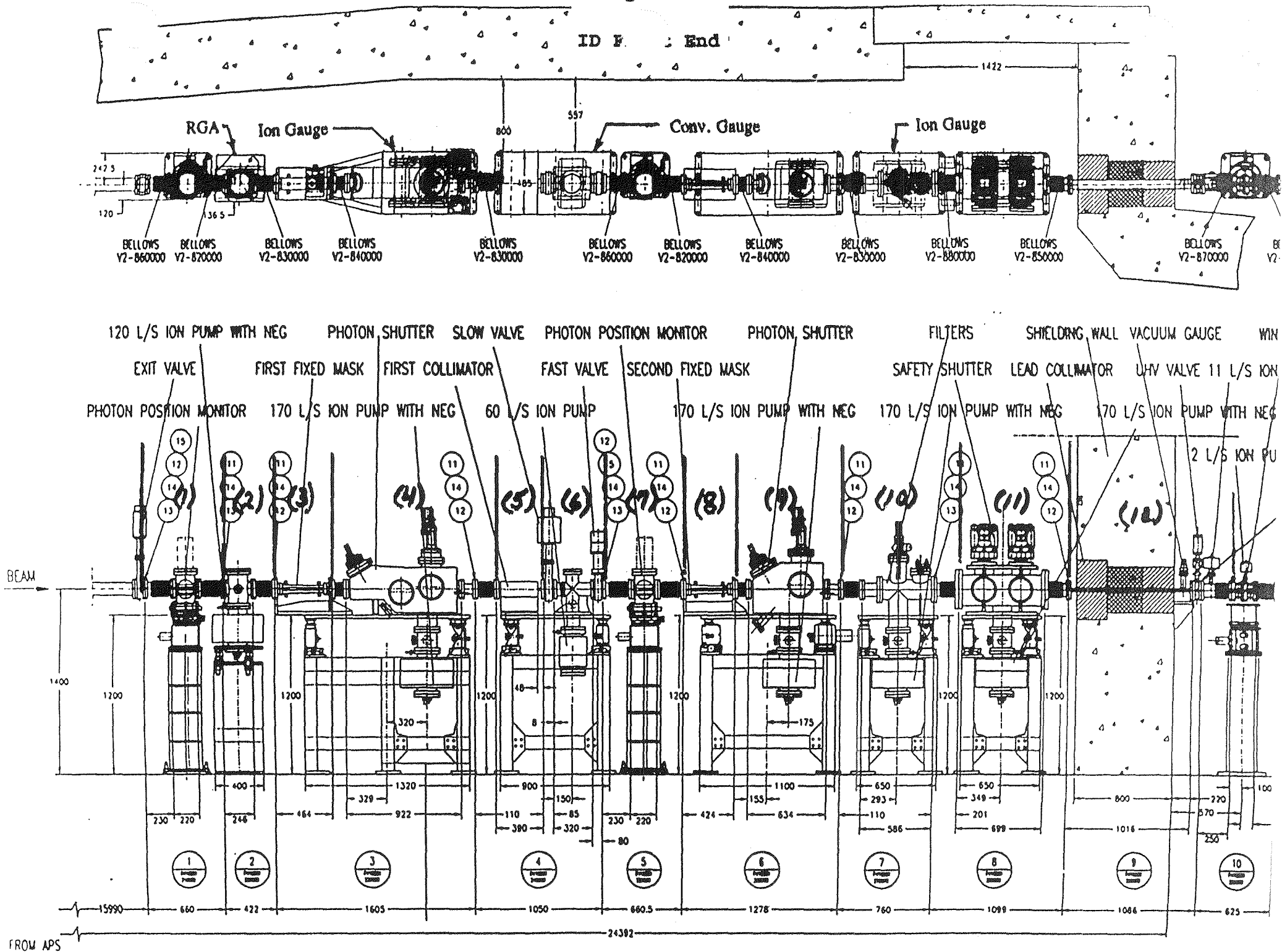
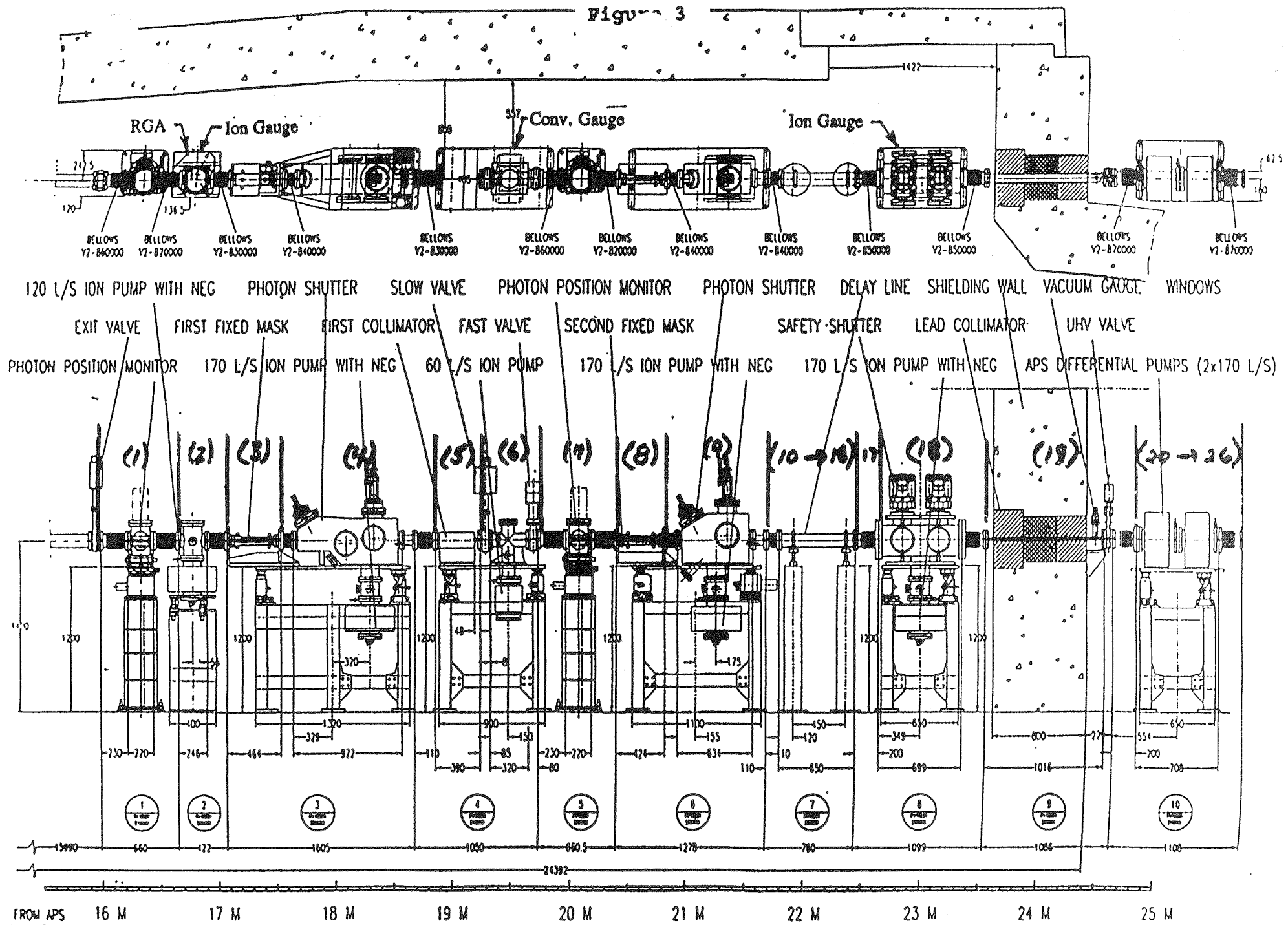
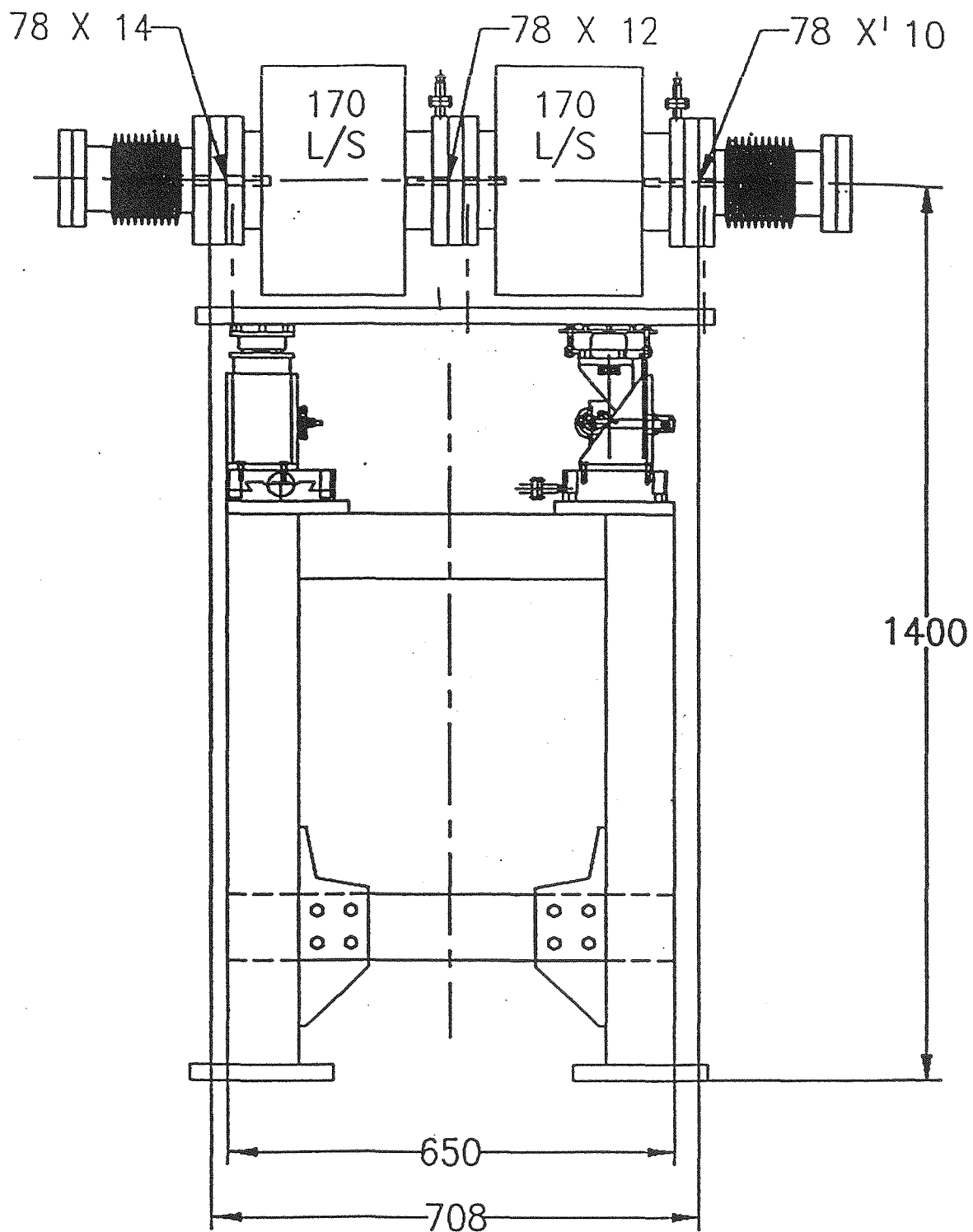


Figure 3



APS INSERTION DEVICE FRONT END GENERAL LAYOUT (WINDOWLESS)

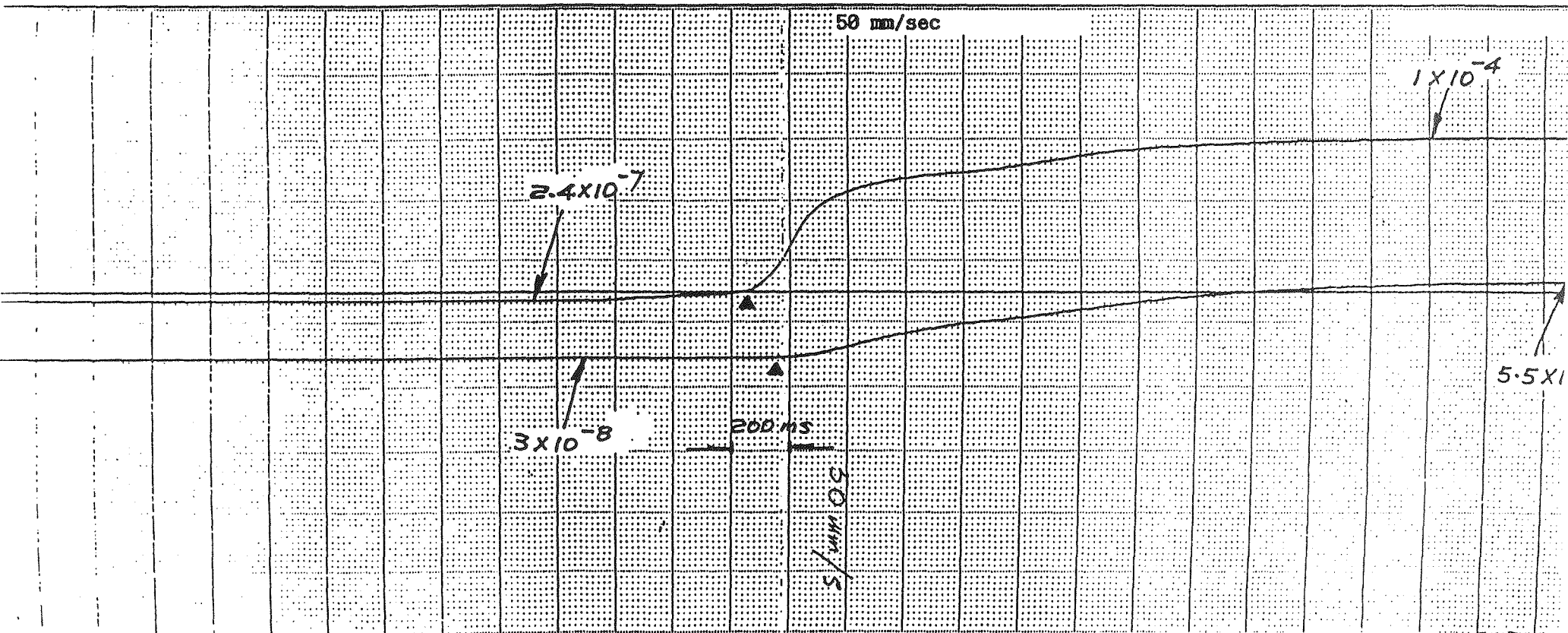
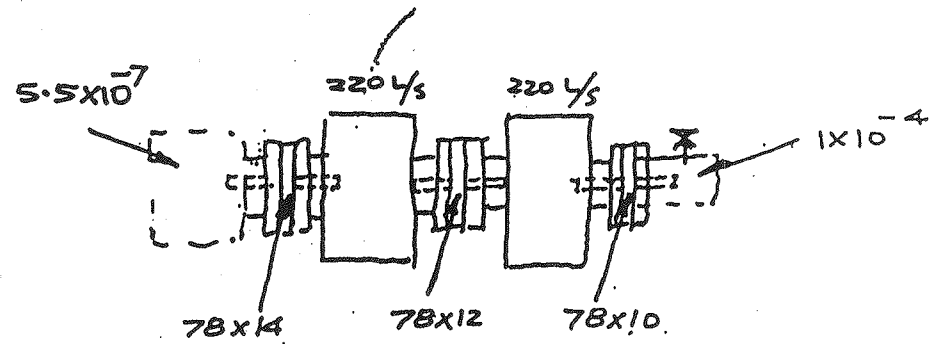


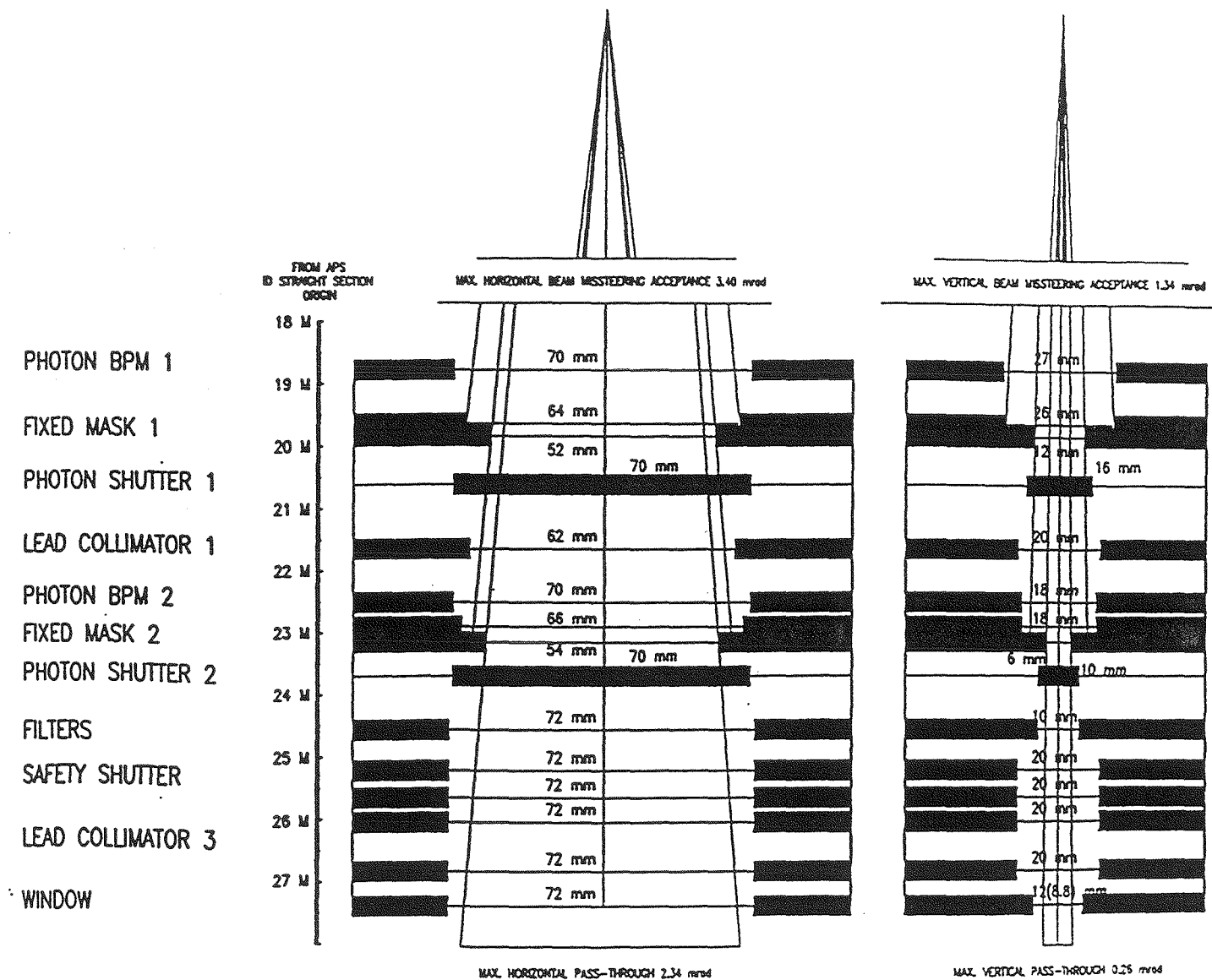
Differential Pump

Figure 4

Figure 5

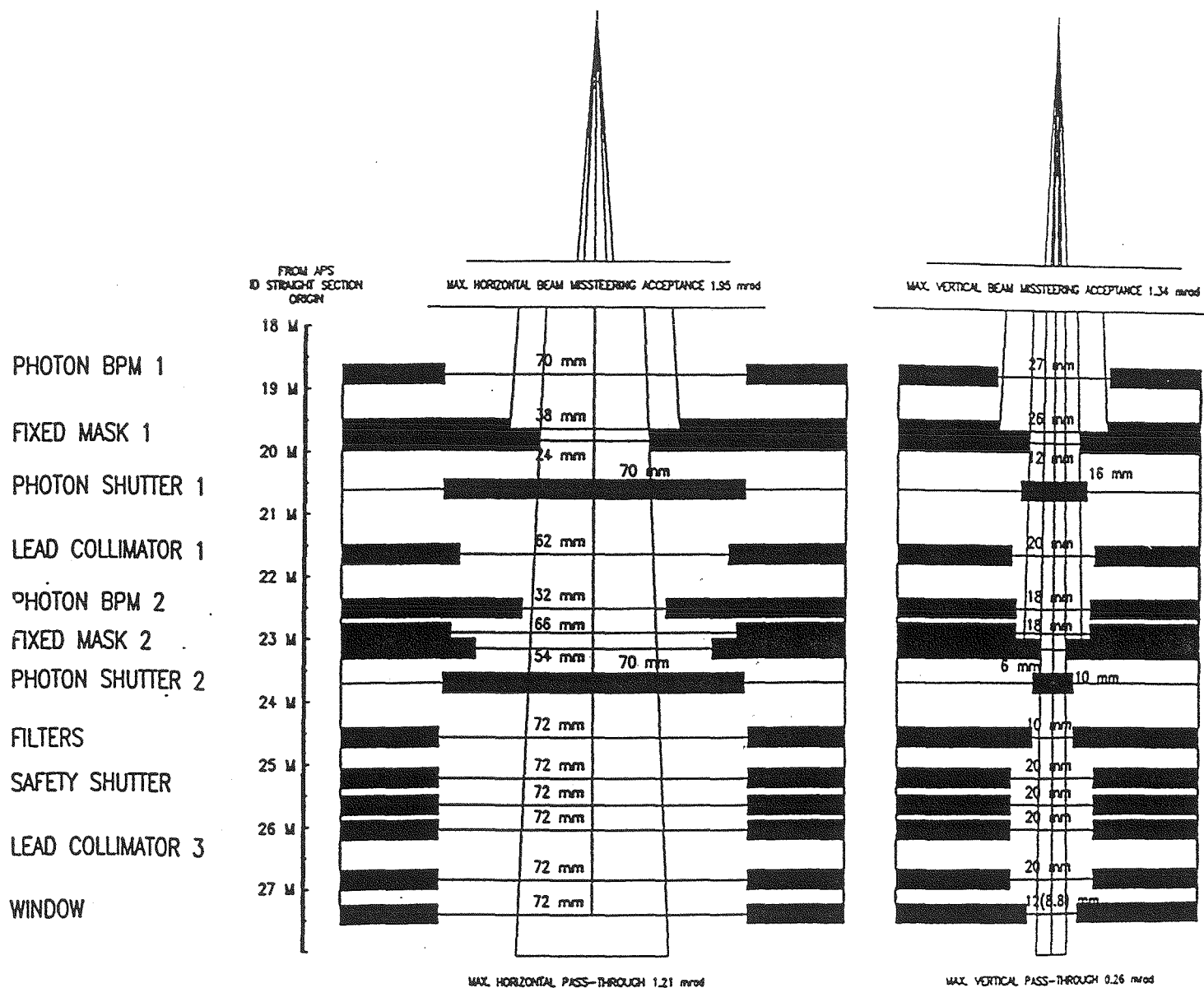
Differential Amp Time Delay





APS ID FRONT END OPTICAL APERTURES

Figure 6



OPTICAL APERTURES FOR APS UNDULATOR FRONT END

Figure 7

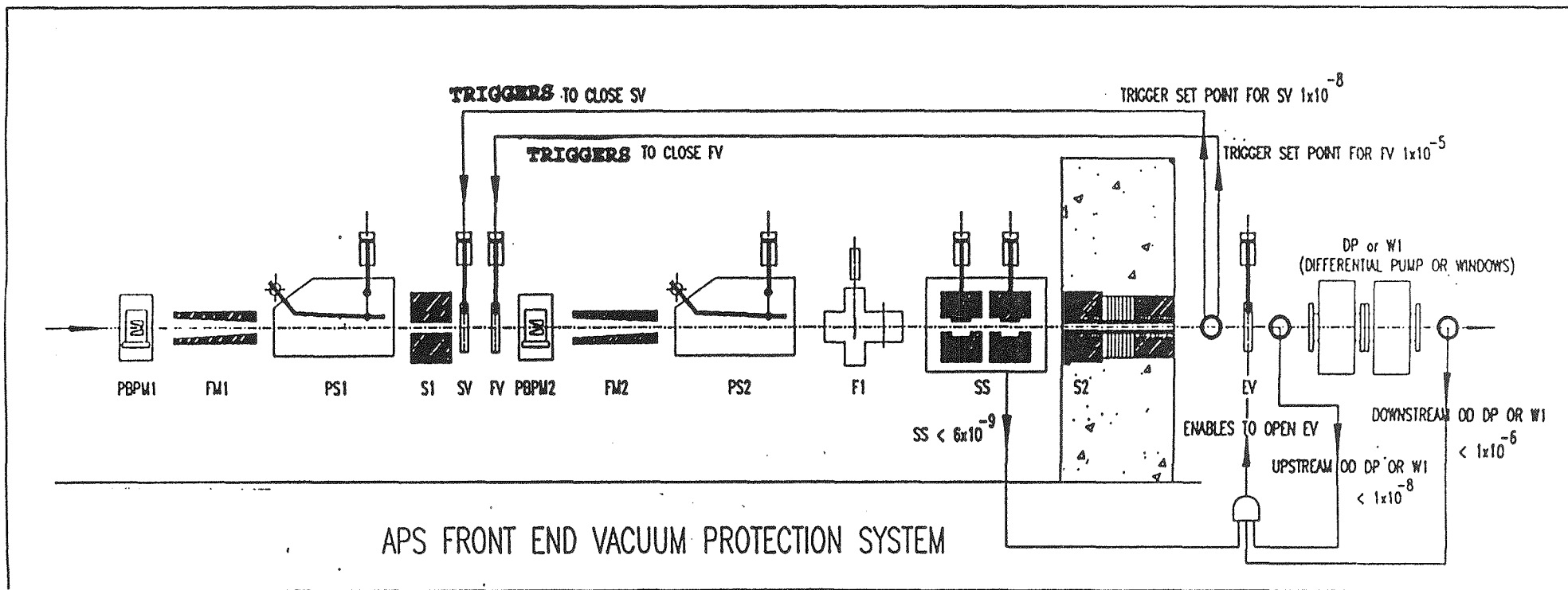
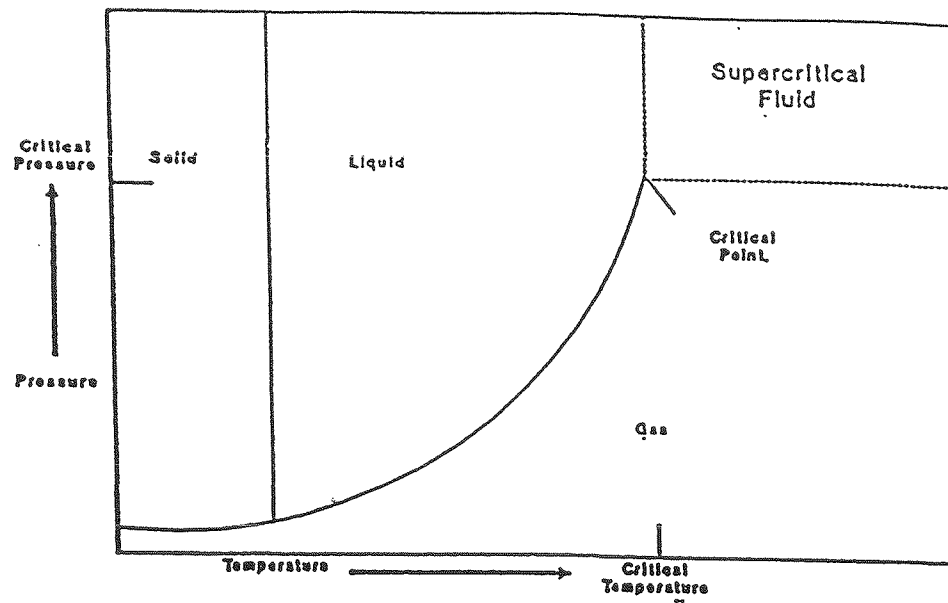
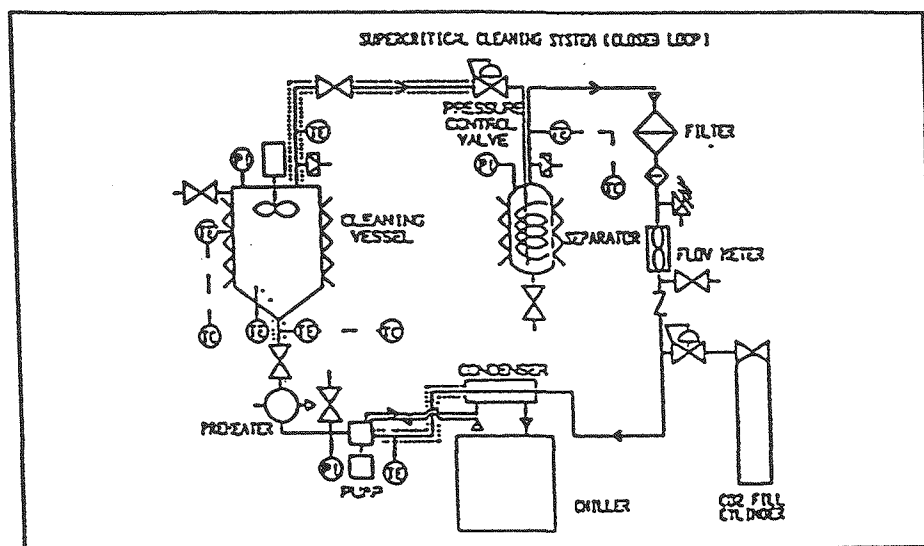


Figure 8



Phase Diagram



Supercritical Cleaning System.

Figure 9

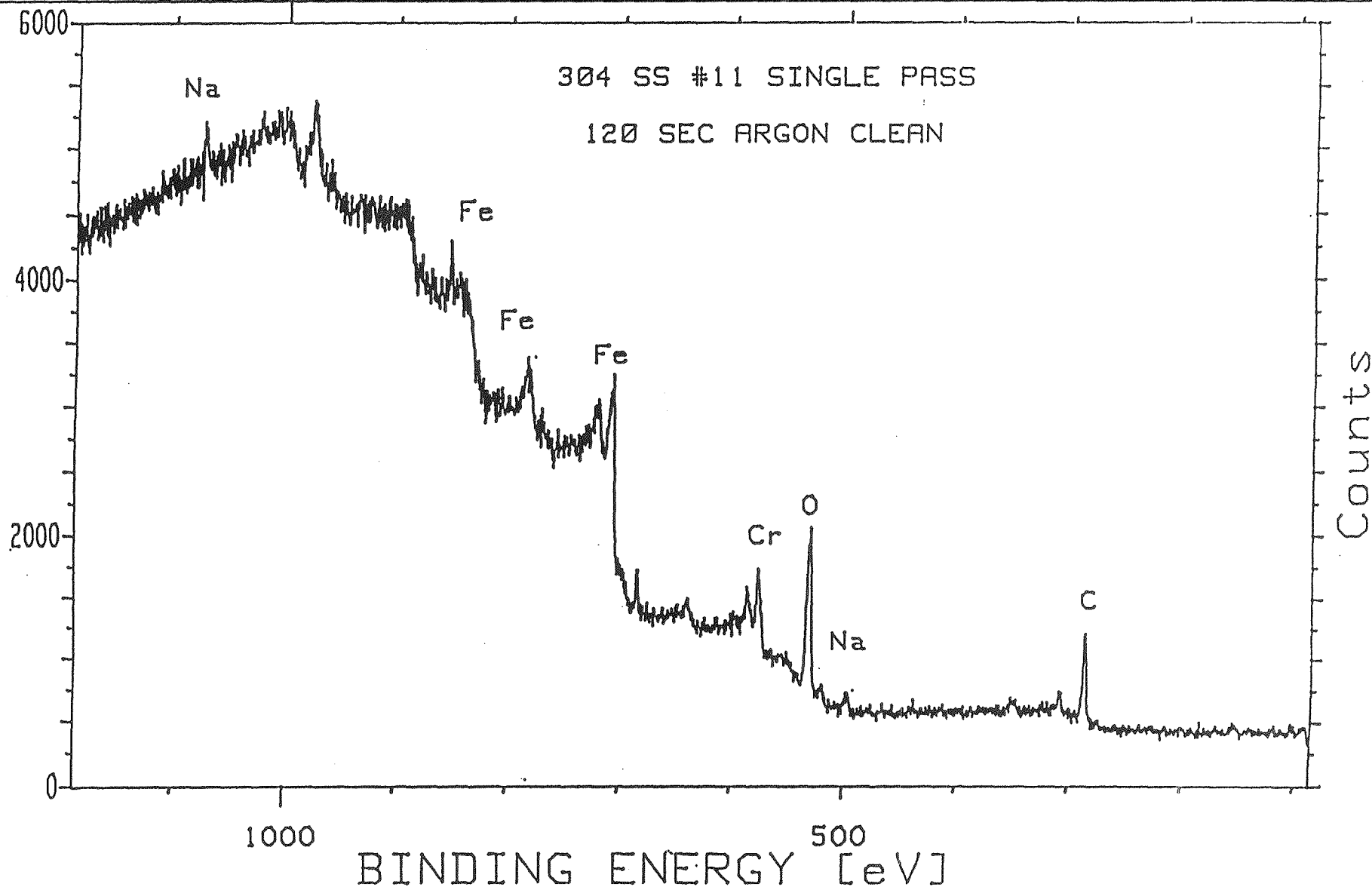


SURFACES
RIBER

ESCA



McCRONE
ASSOCIATES, INC.



Source Power 300 W Step .4

ARGON22_SP

RESO= 1.0eV

Al Anode

16:15:18

6 Apr 1992

Stainless Steel ESCA Profile

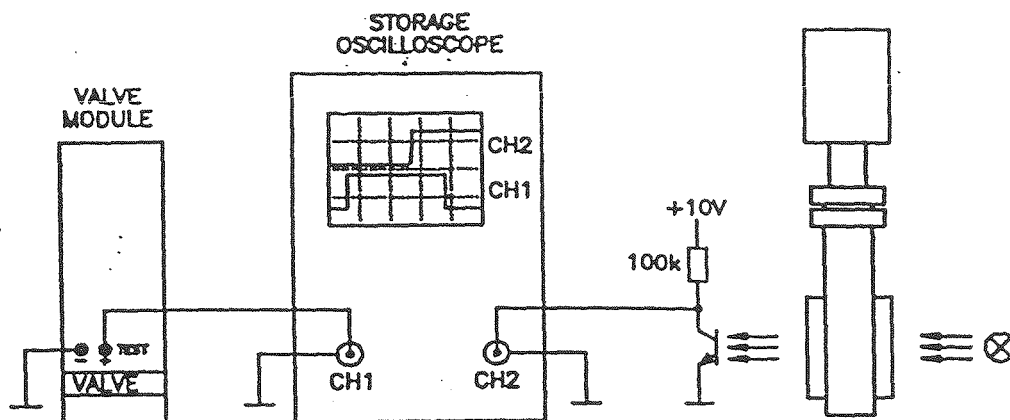
Figure 10

Elemental Atomic Percentages on Sample Surfaces-

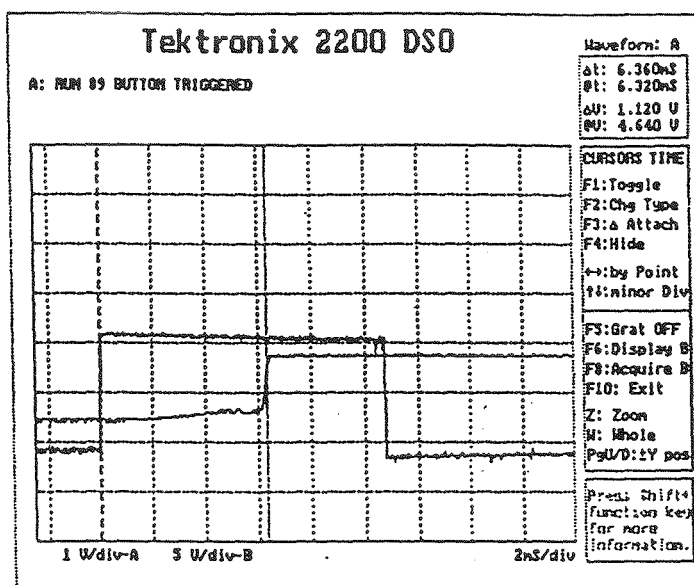
Material	Cleaning Data	Fe	Ni	Cu	Cr	O	C	Ca	Na	Si
304 SS #14	Uncleaned					43.1	51.1		5.7	
304 SS #11	SCC Single Pass	15.3			13	49	19.1		3.6	
Run 1	SCC Single Pass 30 Arg. Cl.	34.5	5.2		16.2	30.9	10.3		2.9	
3500 psi	SCC Single Pass 120 Arg. Cl.	43.8	5.6		13.6	26	7.2	1.3	2.4	
304 SS #12	SCC Single Pass	18	1.2		10.5	46.6	20.2	0.1	3.4	
Run 2	SCC Single Pass 30 Arg. Cl.	33.6	4.5		14.2	31.3	10.6	1.1	4.7	
2000 psi	SCC Single Pass 120 Arg. Cl.	40.8	5.5		15.4	27.8	7.3	0.7	2.5	
304 SS #15	Chemical Clean	42.2	5.1		15.9	30	5.6		1.1	
	Chemical Clean 30 Arg. Cl.	48.6	6.5		14.5	29.4	1			
304L SS #24	Uncleaned					35.5	64.5			
	Uncleaned 120 Arg. Cl.					19.9	72.1		8	
304L SS #21	SCC Single Pass					57.1	31.9		11	
Run 1	SCC Single Pass 30 Arg. Cl.	35.2	4.7		11.6	31.6	12.1		4.8	
3500 psi	SCC Single Pass 120 Arg. Cl.	38.9	5.7		13.5	29.6	6.3	1.6	4.4	
304L SS #23	SCC Single Pass	12.8	1.6		9.9	52.4	19.2		4.1	
Run 2	SCC Single Pass 10 Arg. Cl.	34.5	4.7		9.1	36.2	12.3		3.2	
2000 psi	SCC Single Pass 30 Arg. Cl.	38.9	4.8		10.5	30.2	13.2		2.5	
	SCC Single Pass 120 Arg. Cl.	43.3	5.2		14.7	29.1	5.5		2.2	
304L SS #25	Chemical Clean	31.2	4.2		13.2	42.7	8	0.7		
	Chemical Clean 30 Arg. Cl.	50.6	6.4		13.2	28.6	1.1			
OFHC #5	Uncleaned			65.4		21.3	13.3			
OFHC #1	SCC Single Pass			49		30.6	12.9			7.5
Run 1	SCC Single Pass 30 Arg. Cl.			86.2		8.3	5.5			
3500 psi	SCC Single Pass 120 Arg. Cl.			91.6		4.3	4.1			
OFHC #3	SCC Single Pass			60.5		27.9	11.6			
Run 2	SCC Single Pass 30 Arg. Cl.			91.2		6	2.8			
2000 psi	SCC Single Pass 120 Arg. Cl.			94.4		3.8	1.9			
Material	Cleaning Data	Fe	Ni	Cu	Cr	O	C	Ca	Na	Si
OFHC #6	Chemical Clean			90.8		7	2.2			

Figure 11

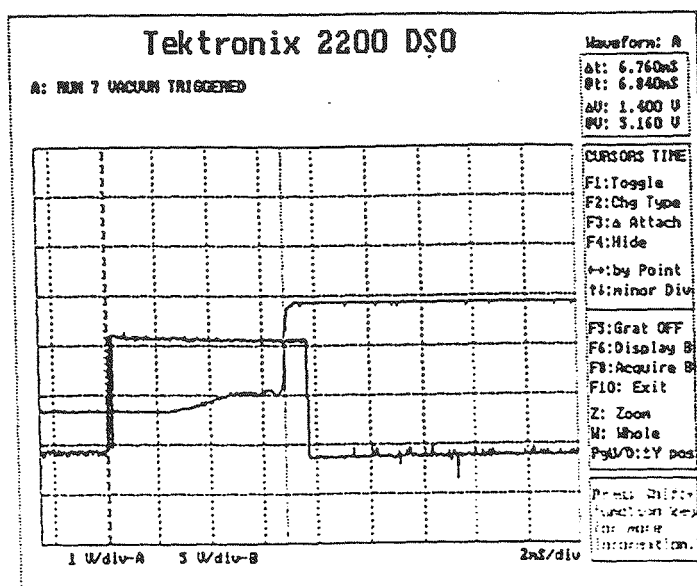
Experimental Setup



Push Button Triggered



Vacuum Triggered



Fast Valve Closing Time

Figure 12